Nonparametric Extraction of Transient Changes in Neurotransmitter Concentration From Dynamic PET Data

Cristian C. Constantinescu*, *Member, IEEE*, Charles Bouman, *Fellow, IEEE*, and Evan D. Morris, *Member, IEEE*

***Abstract*—We have developed a nonparametric approach to the analysis of dynamic positron emission tomography (PET) data for extracting temporal characteristics of the change in endogenous neurotransmitter concentration in the brain. An algebraic method based on singular value decomposition (SVD) was applied to simulated data under both rest (neurotransmitter at baseline) and activated (transient neurotransmitter release) conditions. The resulting signals are related to the integral of the change in free neurotransmitter concentration in the tissue. Therefore, a specially designed minimum mean-square error (MMSE) filter must be applied to the signals to recover the desired temporal pattern of neurotransmitter change. To test the method, we simulated sets of realistic time activity curves representing uptake of [11C]raclopride, a dopamine (DA) receptor antagonist, in brain regions, under baseline and dopamine-release conditions. Our tests considered two scenarios: 1) a spatially homogeneous pattern with all voxels in the activated state presenting an identical DA signal; 2) a spatially heterogeneous pattern in which different DA signals were contained in different families of voxels. In the first case, we demonstrated that the timing of a single DA peak can be accurately identified to within 1 min and that two distinct neurotransmitter peaks can be distinguished. In the second case, separate peaks of activation separated by as little as 5 min can be distinguished. A decrease in blood flow during activation could not account for our findings. We applied the method to human PET data acquired with [11C]raclopride in the presence of transiently elevated DA due to intravenous (IV) alcohol. Our results for an area of the nucleus accumbens—a region relevant to alcohol consumption—agreed with a model-based method for estimating the DA response. SVD-based analysis of dynamic PET data promises a completely noninvasive and model-independent technique for determining the dynamics of a neurotransmitter response to cognitive or pharmacological stimuli. Our results indicate that the method is robust enough for application to voxel-by-voxel data.**

***Index Terms*—Dopamine, positron emission tomography, singular value decomposition.**

I. Introduction

DYNAMIC positron emission tomography (PET) scans with radiolabeled receptor tracers have been used to detect the time-averaged effect of the transient elevation of an endogenous neurotransmitter in response to stimulation. In 1995, Morris *et al.* used a model to predict that the activation of dopamine (DA) could be detected by estimating binding of a reversible tracer such as [11C]raclopride using PET [1], [2]. As DA is released by the presynaptic neuron (i.e., synaptic DA increases), there is increased competition for binding sites between DA and radiotracer, and specific binding of the radiotracer declines.

Subsequent studies were successful in using PET to detect and quantify transient changes in DA following the administration of drugs [3], [4] or a cognitive or motor task [5]–[7]. Most of the PET methods for detecting changes in neurotransmitter concentration have relied on estimation of parameters of a compartmental model, and therefore have been parametric. Apparent change in the compound parameter, binding potential (steady state ratio of bound to free tracer), has been used most often [8], [9]. However, our colleagues have shown recently that this index of change conflates two distinct aspects of neurotransmitter release, magnitude and timing [10]. Extended compartmental models have been created to explicitly account for transient effects of the endogenous neurotransmitter. In one such model proposed by Endres *et al.*, DA changes are accounted for by time-varying kinetic rate constants [11], [12]. They also established mathematical relationships between the measurable parameters of tracer binding and the DA change. Friston *et al.* used a single PET scan design and combined time-dependent compartmental model analysis with linear statistical modeling to detect time dependent displacement of receptor ligands [13]. In a similar approach, Alpert *et al.* linearized a simplified reference region model of Gunn *et al.* [14] and allowed select kinetic parameters to vary in time in order to detect statistically significant DA transients [15]. All of the aforementioned studies were concerned with detection of change in DA, which includes measurement of the magnitude of DA change. However, it is important to recognize that previous measurements of magnitude were a complex average over the whole scan duration. The previous studies were not concerned with temporal characterization of the change.

Because the dynamics of drug-induced increases in DA may be associated with the rewarding properties of drugs of abuse [16]–[18] there would be great value in being able to recover the temporal pattern of DA increases in specific brain regions, or, in other words, in being able to characterize temporally the change in DA concentration.

A parametric approach has recently been proposed by Morris *et al.* [19] to characterize the transient changes in neurotransmitter concentration by extending the standard compartmental

Manuscript received September 8, 2006; revised December 14, 2006. This work was supported by the Whitaker Foundation under Grant RG020126 and Grant TF040034 to E. D. Morris.*Asterisk indicates corresponding author.*

*C. C. Constantinescu is with the Weldon School of Biomedical Engineering, Purdue University, West Lafayette, IN 46907 USA (e-mail: constanc@purdue.edu).

C. Bouman is with the School of Electrical and Computer Engineering and with Weldon School of Biomedical Engineering, Purdue University, West Lafayette, IN 46907 USA (e-mail: bouman@ecn.purdue.edu).

E. D. Morris is with Department of Biomedical Engineering, Indiana University-Purdue University, Indianapolis, IN 46202, USA and also with the Department of Radiology, Indiana University School of Medicine, Indianapolis, IN 46202 USA (e-mail: emorris@iupui.edu).

Digital Object Identifier 10.1109/TMI.2006.891501

models of tracer uptake to include a parameterized description of an endogenous competitor's transient change. However, a nonparametric approach has certain advantages. It is independent of any assumptions about curve shape that describe the time-course of the neurotransmitter. In other words, one need not pre-assume a particular functional form for the change in neurotransmitter over time.

Singular value decomposition (SVD) has proved to be an excellent tool in signal analysis to estimate spatially-independent sources and to extract the signals from noisy data [20]. In functional imaging, SVD is also used in conjunction with principal component analysis (PCA) in multivariate analysis of brain images acquired with PET and fMRI [21]–[24]. The only assumption that one must make is that the system is described by a linear model.

In this work, we describe a SVD-based method for extracting the time profile of the change in free (as opposed to receptor-bound) DA concentration using dynamic PET scans acquired in two conditions: the resting ("R") state and the activated ("A") state (e.g., following pharmacological challenge). The present study seeks to determine the validity of the method for distinguishing distinct neurotransmitter release episodes in time using voxel-based dynamic data.

II. Methods

The implementation and testing of our analysis method consists of three main operations: 1) simulation of realistic PET data based on tracer kinetic parameters previously estimated from experimental data; 2) algebraic manipulation of both "R" and "A" state data using singular value decomposition (SVD) in order to extract components of the PET data that are exclusively related to the neurotransmitter activation; 3) application of a minimum mean square error (MMSE) filter that applies a derivative-like operation to the results of the SVD step, 2.

In the SVD step, we enforce a presumed orthogonality between the signals describing the "R" state and the signals caused by a DA response in the "A" state. We also assume that the signals associated exclusively with the "A" state can, in turn, be entirely explained as linear combinations of distinct temporal features associated with the time-varying neurotransmitter activation.

A. Simulated Data

1) Synthetic PET Time-Activity Curves: PET time-activity curves (TACs) were simulated with a modified version of the standard 2-tissue compartment model [1] which accounted for the release of an endogenous neurotransmitter (e.g., DA) and its competition for available receptor sites with an exogenous tracer (e.g., [11C]raclopride) (see Appendix, Fig. 8). The duration of each PET scan session was assumed to be 60 min, and each time frame was set to 1 min, resulting in $N = 60$ data points per simulated TAC. The tracer kinetics used for this study were those of [11C]raclopride, a dopamine D2/D3 receptor antagonist. The model parameter values (see Appendix) describing the tracer kinetics were selected by fitting the 2-tissue compartment model to experimental data acquired in our laboratory. The parameters for endogenous DA kinetics were chosen from literature [2]. We refer to all these model parameter values as our canonical values. Multiple sets of noisy TACs were generated by repeatedly solving the model with randomly varying tracer parameters, $\overline{\boldsymbol{\theta}}_{\mathrm{tracer}} = [K_1, k_2, k_{\mathrm{on}}, k_{\mathrm{off}}, B_{\max}]$ and adding independent noise realizations. For each generated TAC, $\overline{\boldsymbol{\theta}}_{\mathrm{tracer}}$ was chosen from uniform distributions on an interval $\pm 10\%$ around each canonical value. The association and dissociation rates ($k_{\mathrm{on}}^{\mathrm{DA}}$, $k_{\mathrm{off}}^{\mathrm{DA}}$) of DA at the D2/D3 receptors were not allowed to vary [2]. The resulting curves can be thought of as TACs from M nonidentical regions (i.e., voxels) in the brain with a high amount of specific binding of the tracer to the receptors. In any data set, half the TACs were in the "R" state and half were in the "A" state. In the "A" state, the free DA (F^{DA}) concentration was time-varying.

In the present work, we considered two scenarios for the F^{DA} change in the "A" state: a spatially homogeneous pattern of DA release (i.e., the same F^{DA} time profile for all voxels) and a spatially heterogeneous pattern (i.e., different F^{DA} time profiles at different groups of voxels). In the "R" state, the F^{DA} concentration was kept constant at a baseline value of 100 pmol/ml throughout the scan. The tracer parameters were chosen independently in each condition ("A" or "R"). Gaussian noise was added to the curves according to the model $\sigma^2(t;q) = q_1 + q_2^*(\mathrm{TAC}(t)/\Delta t)q_3$, where $\sigma^2(t;q)$ is the variance at a given time point of the simulated PET image data. $\mathrm{TAC}(t)$ represents the activity concentration at time t, and Δt is the length of the time frame. The parameters $q = [q_1, q_2, q_3]$ were estimated from voxel-based TACs derived from our experimental data acquired during human PET scans with [11C]raclopride. Details are presented in the Appendix C. Using the fitted noise parameters, q, we were able to generate realistic noisy data with a noise level matching that of our experimental data at the voxel level. The % noise at 60 min reached approximately 25% of the mean. At the maximum value of the TAC, it was approximately 6.3% of the mean. Since PET measures the total radioactivity, the TACs were in units of activity concentration (see Appendix B). All TACs were converted from activity/volume units ($\mu\mathrm{Ci/ml}$) to molar concentration units (pmol/ml) and by correcting for radioactive decay and dividing by the specific activity, SA ($\mu\mathrm{Ci/pmol}$) measured at the time of tracer injection. For the sake of simplicity, we will refer to these curves in molar units as "PET signals" for the rest of this text. The signals described in this section were also called "test" signals since we used them to test our method.

2) Null Data: We sought a means of assessing the statistical validity of our recovered signals. To determine the statistical significance of any recovered signals we needed to compare them with recovered signals in the absence of DA activation. We simulated additional "R" and "A" PET signals using the same canonical values for tracer kinetics as for the test signals, except that the F^{DA} was held to 100 pmol/ml throughout both scans. In this case, the data under the two conditions differed only in their noise realizations and in their tracer kinetics. The PET signals generated in this way were called null data. The F^{DA} signals extracted from the simulated null data were referred to as null F^{DA} signals.

3) Endogenous Input Curves, $F^{DA}(t)$: The noiseless time course of F^{DA}, $F^{\mathrm{DA}}(t)$, during the activation was simulated

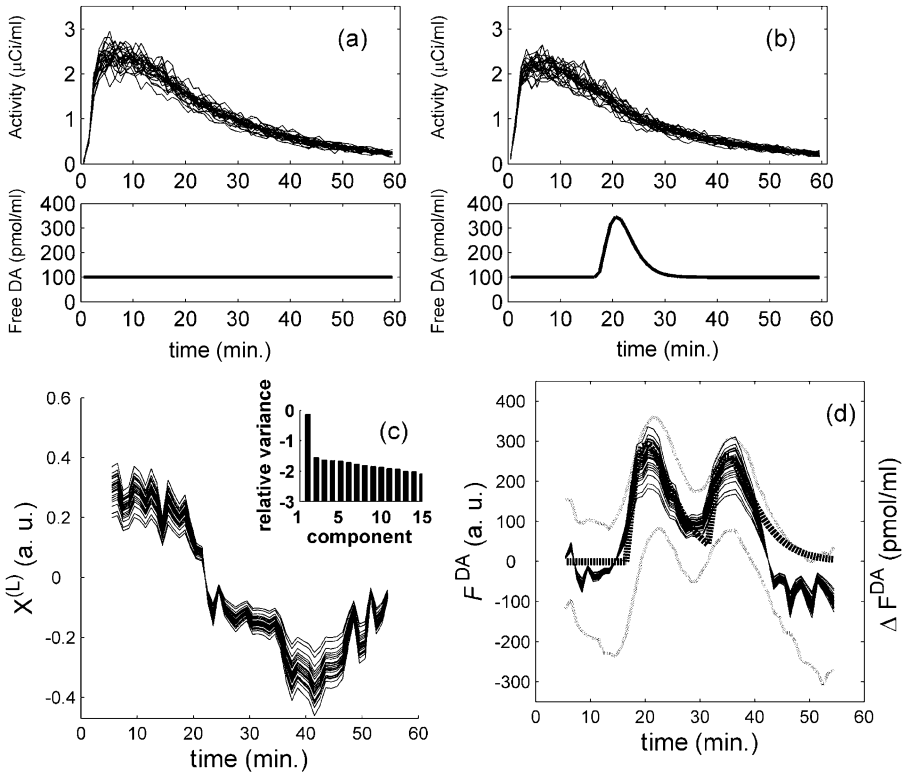

Fig. 1. An example of simulated TACs from 25 different voxels created for "R" and "A" conditions. The TACs were generated with randomly varying tracer kinetic parameters (for [11C]raclopride). Each curve has 60 data points, acquired over 60 min, with 1 min time frames. The data were simulated using the FDA(t) input curves shown below each set of TACs. The curves in the top panel of (a) and (c) represent the simulated data for the unimodal DA activation case and the curves in the top panel of (b) and (d) display the simulated data for the bimodal activation study. The TACs on the left [upper plots of (a) and (c)] were generated under the "R" condition and the curves on the right [upper plots of (b) and (d)] were generated under the "A" condition. The TACs are not corrected for radioactive decay. The flat lines [bottom of (a) and (c)] displayed under the "R" state TACs reflect the assumption that FDA is constant (we used 100 pmol/ml) throughout the rest scan. In the "A" state the FDA(t) curve consisted of either a single gamma-variate function [bottom panel of (b)] for the unimodal activation case, or of two overlapping gamma-variate functions [bottom of (d)] with two peaks separated by 15 min for the bimodal activation.

using gamma-variate functions as follows:

$$F^{\mathrm{DA}}(t) = Basal + \sum_{i=1}^{n} \gamma_i \cdot (t-\tau_i)^{\alpha} \cdot \exp\left(-\beta(t-\tau_i)\right) \quad (1)$$

where n is either 1 or 2 depending on whether the F^{DA} response is unimodal or bimodal, respectively. $Basal$ is the offset parameter (baseline DA concentration), α defines the curve's power ascent, β defines the curve's exponential descent, γ_{i} are the magnitude coefficients, and τ_i represent the delay between the start of the scan and the initiation of the ith response. The ratio α/β defines the time at which the curve reaches its peak value. We introduce the notation $\overline{\theta}_{\mathrm{DA}} = [\mathrm{Basal}, \alpha, \beta, \gamma, \tau]$ for the entire set of DA parameters. In all simulated cases, the responses start after the [11C]raclopride injection ($\tau > 0$). To simulate a homogenous DA activation we used either, a unimodal response [see Fig. 1(b)], or a bimodal response [see Fig. 1(d)] with an offset parameter. The values of $\overline{\theta}_{\mathrm{DA}}$ for the two types of responses are given in Table I. The rationale for the use of the gamma-variate function was based on observations from microdialysis on nonhuman primates and rodents that have shown various DA responses characterized by a rise and then a fall in DA concentration, reasonably described by a gamma-variate function [25]–[27].

TABLE I
TRUE PEAK POSITIONS AND THE MEAN DETECTED POSITIONS FOR TWO DIFFERENT SIMULATED CASES OF SPATIALLY HOMOGENEOUS DA ACTIVATION. THE STANDARD DEVIATIONS ARE GIVEN IN PARENTHESIS. THE PARAMETERS [SEE (1)] THAT DEFINE THE TRUE F^{DA} RESPONSES ARE GIVEN FOR EACH CASE

Case:	1. Unimodal	2. Bimodal
True F^{DA} parameters	Basal = 100 pmol/ml α= 2.6, β=0.7, (α/β=3.7) τ=16.8 min, γ=100	Basal = 100 pmol/ml α= 1.0, β=0.3, (α/β=3.3) τ_1=16.8 min, τ_2=31.8 min γ_1=240, γ_2=200
True peak times (min)	20.7	23.8 35
Detected peak	21.7 (1.2)	22.3 (1.6)

To simulate an heterogeneous pattern of DA activation across voxels, the F^{DA} was simulated as follows:

$$F^{\mathrm{DA}}(t;j) = Basal + \gamma(j)\,(t-\tau(j))^{\alpha} \cdot \exp\left(-\beta\,(t-\tau(j))\right) \quad (2)$$

where j can take on different values corresponding to different classes of PET signals. In our simulations, we combined four classes of signals, three differed in their time delay $\tau(\mathrm{j})\,\mathrm{j} \in [1,3]$

TABLE II
TRUE PEAK POSITIONS AND THE MEAN DETECTED POSITIONS FOR THREE DIFFERENT SIMULATED CASES OF SPATIALLY HETEROGENEOUS DA ACTIVATION. THE STANDARD DEVIATIONS ARE GIVEN IN PARENTHESIS. THE PARAMETERS [SEE (2)] THAT DEFINE THE TRUE F^{DA} RESPONSES ARE GIVEN FOR EACH CASE

Case:	1. Robust activation	2. Mild activation	3. Mild activation – 10 min separation
True F^{DA} parameters [a]	τ(1)=20 min,τ(2)=25 min, τ(2)=30 min γ(1)= γ(2)= γ(3)=300, γ(4)=0	τ(1)=20 min,τ(2)=25 min, τ(2)=30 min γ(1)= γ(2)= γ(3)=100, γ(4)=0	τ(1)=20 min,τ(2)=30 min, τ(2)=40 min γ(1)= γ(2)= γ(3)=100, γ(4)=0
True peak times (min)	23.8 28.8 33.8	23.8 28.8 33.8	23.8 33.8 43.8
Detected peak times (min)	26.0 (0.7) 30.7 (0.8) 34.4 (0.9)	26.3 (0.5) 30.8 (0.9) 34.0 (1.0)	25.6 (0.9) 34.8 (0.9) 44.7 (1.3)

[a]The parameters *Basal,* α, and β are the ones used for unimodal case (see Table I)

and the fourth was comprised of only the $Basal$ concentration $(\gamma(4) = 0)$. The first three classes represent true DA activation. The fourth class simulates the *null* DA activation. The parameters of $F^{\mathrm{DA}}(t; j)$ used in our simulations are given in Table II.

4) Exogenous Input, $P(t)$*:* The delivery of tracer to the tissue is governed by the time-varying concentration of tracer in the plasma compartment, $P(t)$ [see Appendix, (A1)–(A3)], also known as the exogenous input function. For our simulations, we used bolus delivery as our exogenous inputs. Data from actual blood samples measured during experiments with [11C]raclopride (described in the next section) were used. Although the radioactivity concentration was measured in arterial blood, realistic (molar) plasma curves were constructed from arterial blood curves by assuming a specific activity (SA) value of 1 $\mu\mathrm{Ci/pmol}$ and a constant hematocrit of 39%.

B. Experimental Test Data

The experimental data that we used to test our method were acquired from one human subject in an ongoing research study. The experimental protocol is described in detail elsewhere [28]. In brief, the first scan was in the "R" state: the subject was scanned while resting (eyes open) in the scanner. The second scan was an "A" scan: the subject was shown visual cues related to alcohol, exposed to odors of alcohol beverages, and administered alcohol intravenously with the intent of provoking a dopaminergic response. Dynamic PET data were acquired (ECAT EXACT HR+ PET scanner), following administration of 15.93 mCi (first scan) and 16.64 mCi (second scan) of [11C]raclopride. The tracer specific activities at time of injection were 1.173 $\mu\mathrm{Ci/pmol}$ and 1.234 $\mu\mathrm{Ci/pmol}$, respectively. The cues were shown starting 2 min before the tracer injection. The intravenous infusion of alcohol started at 3 min post-[11C]raclopride injection, reached the target of 60 mg% breath alcohol concentration (BrAC) after 10 min and was clamped at this BrAC (±5 mg%) for 30 min [29], [30]. The total duration of each dynamic scan was 60 min, and was made up of 61 acquisition frames (10 × 30 s, 50 × 1 min, and 1 × 5 min). The images were reconstructed using filtered backprojection with a 5 mm Hanning filter. Full-width at half-maximum (FWHM) was 9 mm. The subject also received a T1-weighted MR image with a 1.5T GE Echospeed LX scanner. The PET images were motion-corrected using the SPM2[1] package by co-registration of each image to an early (10 min) summed image. The summed PET image was then co-registered to the subject's MR scan and the resulting transformation matrix was applied to each PET image. The MR image was normalized to a standard MNI space and the resulting transformation matrix was applied to the motion-corrected, co-registered PET data. The final voxel size of the transformed PET images was $2\ \mathrm{mm} \times 2\ \mathrm{mm} \times 2\ \mathrm{mm}$. Twenty-four spherical regions of interest (ROI) were drawn on three major regions of the basal ganglia: the Nucleus Accumbens (NAcc) (12 ROIs, 264 mm^3 each), the putamen (6, 648 mm^3), and the caudate nucleus (6, 648 mm^3), divided equally between the two hemispheres of the brain. NAcc is known as an area of the brain prone to DA activation in response to rewarding stimuli [27], [31], [32].

The 24 ROIs were then projected onto the 61 dynamic PET images. TACs were constructed using the average signal in each ROI over each timeframe. The TACs were decay corrected and then converted to molar quantities. All data were interpolated using cubic splines to 1 min frames since, as currently configured, the present application requires data sampled at equally-spaced time intervals. Usable curves were limited to the first 55 min of scan duration since the last image in the dynamic series was taken over 5 min, and could not be used.

In addition to the method described in the next section, the F^{DA} time profile was estimated from a model-based method, $nt\mathrm{PET}$, as introduced in [19]. Briefly, the $nt\mathrm{PET}$) method employs the enhanced tracer kinetic model (Appendix, Fig. 8) that describes the uptake of a D2/D3 tracer in the presence of a time-varying change in DA. This change is assumed to be described by a gamma-variate function, whose parameters are estimated from fitting the model to all the data (i.e., both conditions) simultaneously using a constrained, weighted objective function. As with the current method, $nt\mathrm{PET}$ requires data acquired during rest and activation (transient DA change) conditions.

C. Mathematical Algorithm

1) SVD Analysis: We use convenient matrix notation to represent the data. The "A" and "R" PET signals were collected, respectively, into two $N \times M$ matrices $\boldsymbol{A}$ and $\boldsymbol{R}$. In each matrix, the number of columns, M, equals the number of PET signals. The number of rows, N, equals the number of time samples in

[1]http://www.fil.ion.ucl.ac.uk /spm

each signal. The SVD [20] of $\boldsymbol{R}$ is given by the following matrix equation:

$$\boldsymbol{R} = \boldsymbol{U}_R \cdot \boldsymbol{S}_R \cdot \boldsymbol{V}_R \tag{3}$$

where $\boldsymbol{U}_R$ is an $(N \times M)$ orthonormal matrix with columns representing the left singular vectors in the "R"-signal space, $\{\boldsymbol{U}_{R_i}\}_{i=1,\ldots M}$, $\boldsymbol{V}_R$ is a $M \times M$ orthonormal matrix with columns representing the right singular vectors in the time samples space $\{\boldsymbol{V}_{R_i}\}_{i=1,\ldots M}$ and $\boldsymbol{S}_R$ is a $M \times M$ diagonal matrix containing the singular values of $\boldsymbol{R}$, $\{\boldsymbol{S}_{R_i}\}_{i=1,\ldots M}$.

We assume, without loss of generality, that the number of signals is smaller than the number of samples (i.e., $M \leq N$). Following the Matlab convention, we used the *economy size* decomposition, which means that only the first M columns of matrix $\boldsymbol{U}_R$ are computed, and $\boldsymbol{S}_R$ is $M \times M$, instead of commonly seen $N \times N$.

After decomposing the matrix $\boldsymbol{R}$ according to (3), we form a new lower dimensional representation of $\boldsymbol{U}_R$, designated $\boldsymbol{U}_R^{(K)}$, which is an $(N \times K)$ matrix whose K columns contain the most significant singular vectors in the "R"-signal space, $\{\boldsymbol{U}_{R_j}^{(K)}\}_{j=1,,\ldots K}$. A *scree* plot [33] of relative variances $(S_{R_i}^2 / \sum_{i=1}^{M} S_{R_i}^2)$ is used for determining the number of significant vectors, K, to be retained in matrix $\boldsymbol{U}_R^{(K)}$. Next, we find the vectors that are unique to the "A" state. Effectively, we *subtract* the "R" state contribution from the "A" state signals, by projecting onto the subspace described by the K orthonormal vectors $\{\boldsymbol{U}_{R_j}^{(K)}\}$ of the reduced "R" space and then subtracting that projection from matrix, $\boldsymbol{A}$. The result is a new $(\mathrm{N} \times \mathrm{M})$ matrix

$$\boldsymbol{X} = \left(\boldsymbol{I} - \boldsymbol{U}_R^{(K)} \cdot \boldsymbol{U}_R^{(K)^T}\right) \cdot \boldsymbol{A} \tag{4}$$

where $\boldsymbol{I}$ is the $(N \times N)$ identity matrix $\boldsymbol{X}$. The matrix is further decomposed as

$$\boldsymbol{X} = \boldsymbol{U}_X \cdot \boldsymbol{S}_X \cdot \boldsymbol{V}_X^T \tag{5}$$

where $\boldsymbol{U}_X$ and $\boldsymbol{V}_X$ are matrices containing the left and right singular vectors, $\{\boldsymbol{U}_{X_i}\}_{\mathrm{i}=1,,\ldots \mathrm{M}}$, and $\{\boldsymbol{V}_{X_i}\}_{i=1,,\ldots \mathrm{M}}$; $\boldsymbol{S}_X$ is the diagonal matrix containing the singular values. We will refer to the signals held in $\boldsymbol{X}$ as the *difference* signals. The matrix $\boldsymbol{X}$, representing the difference between rest and activation, is further replaced by the closest rank-L matrix to $\boldsymbol{X}$ in a least squares sense that would only retain the components associated with activation while eliminating those considered to be noise. The criterion for choosing the L components was, again, based on the analysis of the *scree* plot of relative variances $(S_{X_i}^2 / \sum_{i=1}^{M} S_{X_i}^2)$. The new reduced rank matrix $\boldsymbol{X}^{(L)}$ is given by

$$\boldsymbol{X}^{(L)} = \boldsymbol{U}_X^{(L)} \cdot \boldsymbol{S}_X^{(L)} \cdot \boldsymbol{V}_X^{(L)^T} \tag{6}$$

$\boldsymbol{X}^{(\boldsymbol{L})}$ is an $N \times M$ array that retains the most significant components of the PET signals that can be attributed to activation. Matrices, $\boldsymbol{U}^{(L)}$, $\boldsymbol{S}_X^{(L)}$, and $\boldsymbol{V}_X^{(L)}$ are truncated versions of, $\boldsymbol{U}_X$, $\boldsymbol{S}_X$, and $\boldsymbol{V}_X$, obtained by retaining only the largest L singular values and the singular vectors that correspond to them. We will refer to the signals held in $\boldsymbol{X}^{(L)}$ as the *activation* signals.

2) Scree Plot Analysis: Following the decomposition in (3) and (5), we used the *scree* plot combined with a statistical method for objectively deciding which components represent the structured signal and which are associated with noise.

The *scree* plot, which sorts the components' relative variances in the order of importance, typically drops, then reaches a turning point and finally levels off. Using a semi-logarithmic scale, we retained the number of components preceding the turning point and discarded the rest, which we considered to represent noise. In order to determine the position of the turning point, we employed a novel discrimination method. We assumed that the variances associated with the noise should follow a straight line in the *scree* plot and treat the variances associated with the structured signals as "outliers" from that line. Let $\{p_i\}_{i=1,\ldots M}$, be the base 10 logarithm of relative variances, represented on the *scree* plot. The following steps were followed to determine the number of significant singular values.

Step 1) Fit a line to the last (smallest) q values, $\{p_i\}_{i=M-q+1,,\ldots M}$;

Step 2) Use the regression line parameters to predict the value of the $(M\text{-}q)$th component, $\overline{p}_{M-q}$;

Step 3) Calculate a z-score for the $(M\text{-}q)$th component;

$$Zscore = |p_{M-q} - \overline{p}_{M-q}| / \sqrt{\sum_{i=M-q+1}^{M} (p_i - \overline{p}_i)^2 / (q-l)}$$

where $\{\overline{p}_i\}$ are the values predicted by the regression line.

Step 4) If $Zscore > 3$ declare p_{M-q} an outlier. This is equivalent to saying that the p_{M-q} does not follow the linear trend set by the last q components (i.e., those associated with the noise).

Step 5) Increase q by 1 and repeat Step 1) to Step 4)

The first components that satisfy the z-score criterion are taken to be significant. We used a starting value for q equal to $(2/3) \cdot M$, rounded up towards nearest integer.

3) MMSE Filter Design: The signals $\{\boldsymbol{X}_i^{(L)}\}_{i=1,\ldots \mathrm{M}}$ associated with each voxel i and held in the columns of matrix $\boldsymbol{X}^{(L)}$ must be further processed to yield the desired output, namely the time-courses of *change* in free endogenous dopamine, $\boldsymbol{F}^{\boldsymbol{DA}}(t)$. Preliminary work with idealized $F^{\mathrm{DA}}(t)$ curves (e.g., a delta function) led to the observation that the activation signals $\{\boldsymbol{X}_i^{(L)}\}$ are related to a time integral of $F^{\mathrm{DA}}(t)$ at every voxel. In other words

$$\boldsymbol{X}_i^{(\boldsymbol{L})} = C_i(\theta_{\mathrm{tracer}}) \cdot \left\{ \int_0^t \boldsymbol{F}^{\boldsymbol{DA}}(t')dt' \right\}_i \tag{7}$$

where $C_i(\theta_{\mathrm{tracer}})$ is a scale factor that depends mostly on the tracer kinetic parameters. The integration in (7) is an operation

on column, i, of matrix $\boldsymbol{F}^{\boldsymbol{DA}}(t)$. Said another way, differentiation of the columns of $\boldsymbol{X}^{(\boldsymbol{L})}$ with respect to time yields the time profiles of $F^{\mathrm{DA}}(t)$ at each voxel included in the analysis. Since an increase in DA concentration leads to a decrease in tracer binding, a change of sign is also required. With this in mind, the estimates of the $\boldsymbol{F}^{\boldsymbol{DA}}(t)$ are formally given up to a scale factor by

$$\hat{\boldsymbol{F}}^{\mathrm{DA}}(t) \approx -\frac{d\boldsymbol{X}^{(L)}}{dt} \tag{8}$$

where $\hat{\boldsymbol{F}}^{\boldsymbol{DA}}(t)$ is an $(N \times M)$ matrix with the columns $\{\hat{\boldsymbol{F}}_i^{\mathrm{DA}}(t)\}_{i=1,\ldots M}$, representing the *estimated* F^{DA} signals. We note that our $\hat{\boldsymbol{F}}^{\mathrm{DA}}(t)$ estimate does not contain any information on baseline concentration of F^{DA} in the "A" state since the baseline DA level is common to both "R" and "A" states. Therefore, $\hat{\boldsymbol{F}}^{\mathrm{DA}}(t)$ must be considered an estimate of the *change* in F^{DA}. Theoretically, this change could be either negative or positive. In order to perform the action in (8), which consists of a differentiation-like operation plus a change in sign, the signals in the columns of matrix $\boldsymbol{X}^{(\boldsymbol{L})}$ were filtered with a MMSE linear filter [34]. The filter minimizes the mean square error between the desired signal $\boldsymbol{F}^{\boldsymbol{DA}}(t)$ and the estimated signal, $\hat{\boldsymbol{F}}^{\boldsymbol{DA}}(t)$ through the selection of optimal filter parameters, $\hat{\boldsymbol{\theta}}$. The filter parameters, $\hat{\boldsymbol{\theta}}$, are given by the following vector:

$$\hat{\boldsymbol{\theta}} = arg\,\min_{\theta} \sum_{s=l}^{N_s} \left[\left| \boldsymbol{F}_s^{\mathrm{DA}} - \hat{\boldsymbol{F}}_s^{\mathrm{DA}} \right|^2 \right] \tag{9}$$

where $\boldsymbol{F}_{\boldsymbol{s}}^{\mathbf{DA}}$ represents the value at the discrete time, s, of the desired signal $F^{\mathrm{DA}}(t)$ from a voxel i, and $\hat{F}_s^{\mathrm{DA}} = \boldsymbol{z}_s \cdot \boldsymbol{\theta}$ is the value at time s of the estimate $\hat{\boldsymbol{F}}^{\boldsymbol{DA}}(\boldsymbol{t})$ from the same voxel, $\boldsymbol{z}_s$ is a row vector made from samples in a symmetric window $[x_{s-p,i}^{(L)}, x_{s-p+1,i,,\ldots\ ldots}^{(L)} x_{s,i,,\ldots\ ldots}^{(L)}, x_{s+p-1,i}^{(L)}, x_{s+p,i}^{(L)}]$ surrounding the sample $x_{s,i}^{(L)}$, of the signal $\boldsymbol{X}_i^{(L)}$ associated with the voxel i, and N_S is the total number of time samples from all signals used for the filter training. The filter vector $\hat{\boldsymbol{\theta}}$ contains $2\mathrm{p}+1$ parameters, where p is half the width of the filter. The MMSE filter parameters were derived from a training data set consisting of solutions of the SVD step ($\boldsymbol{X}^{(\boldsymbol{L})}$ signals) and noiseless, but fully characterized $F^{\mathrm{DA}}(t)$ functions (see below).

D. MMSE Filter Training

Training of the filter with simulated data was required to select $\hat{\theta}$. The training data consisted of 10 000 ($F^{\mathrm{DA}}(t)$, $\boldsymbol{X}_i^{(L)}$) signal pairs. This required $N_T = 1000$ noisy simulations (trials) of $M = 10$ ("A" and "R") PET signal pairs. We refer to these signals as training signals, to distinguish them from the test signals, explained earlier. The training PET signals were made of 60 (i.e., $N = 60$) 1-min time samples. Similar to the analysis of the test data with homogeneous activation, all M noisy PET signals were solutions of the model (Appendix, Fig. 8) using a noiseless, analytically described $F^{\mathrm{DA}}(t)$ curve. The $F^{\mathrm{DA}}(t)$ curve was a unimodal function given by parameters $\overline{\boldsymbol{\theta}}_{\mathbf{DA}}$. With each trial, a unique set of parameters$\overline{\boldsymbol{\theta}}_{\mathbf{DA}}$, were drawn from a uniform distribution around the mean values: $\overline{\boldsymbol{\theta}}_{\mathbf{DA}} = [100 \pm 0\%, 1.0 \pm 10\%, 0.3 \pm 20\%, 500 \pm 10\%, 30\,\mathrm{min} \pm 20\%]$. The resulting set of unimodal $F^{\mathrm{DA}}(t)$ curves had different heights and widths spanning the scan duration. The kinetic parameters used to generate PET data for filter training were drawn from the same distribution as the parameters used for the synthetic PET data used as test signals. We chose the tracer parameters to simulate realistic intrasubject and intersubject variability. In addition to the $\pm 10\%$ within trial (akin to intrasubject) variability for the tracer kinetic parameters, $\overline{\boldsymbol{\theta}}_{\mathrm{tracer}}$, we introduced an additional $\pm 20\%$ inter-trial (akin to intersubject) variability. The activation signals, $\boldsymbol{X}^{(\boldsymbol{L})}$ associated with F^{DA} activation were extracted from the simulated PET signals by using (3)–(6). All $\boldsymbol{X}^{(\boldsymbol{L})}$ signal estimates and their desired counterparts, $F^{\mathrm{DA}}(t)$, were used to estimate the optimal filter parameters, $\hat{\boldsymbol{\theta}}$ [see (9)]. The number of trials, N_T, was chosen to be large enough to ensure that the filter was not undertrained. An estimated filter with a fixed kernel size was applied to all test signals presented in the Results section. Adaptive kernel sizes were used at the ends of each signal to avoid having to pad the signal.

E. Correlation Plot Analysis

In the case of simulations with heterogeneous DA activation, we also used correlation scatter plots as an indication that each of the extracted signals was associated with a unique temporal feature [35]. The signals were sorted based on similarity in temporal pattern shown by the left singular vectors, $\{\boldsymbol{U}_{X_i}\}_{i=1,\ldots M}$ from (5). The correlations of the first singular vector, $\boldsymbol{U}_{X_1}$ with each signal $\boldsymbol{X}_i$, $corr(\boldsymbol{U}_{X_1}, \boldsymbol{X}_i)$, were plotted versus the correlations of the second singular vector $\boldsymbol{U}_{X_2}$ with each signal $\boldsymbol{X}_i$, $\mathrm{corr}(\boldsymbol{U}_{X_2}, \boldsymbol{X}_i)$.

F. Effects of CBF Change

We also tested for evidence that the extracted signals could be caused by a decrease in CBF, absent any true DA activation. If CBF is lower during the "A" scan, K_1 and k_2, will be lower and may cause a false positive result. In order to asses the impact of a drop in CBF on our ability to detect changes in F^{DA}, we simulated a "flow-change only" case. In this case, the "A" PET signals were characterized by a 20% drop in the mean K_1 parameter and 10 % drop in mean k_2 starting at 16.5 min after the beginning of the scan, but no DA change. K_1 and k_2 are both functions of CBF. Although it is unlikely that K_1 and k_2 would change disjointly, it has been shown previously that change in K_1 and k_2 without changing the distribution volume, $V_D (= K_1/k_2)$, has little or no effect on PET curve shape [6], [15]. Nevertheless, to check the effect of equal change in K_1, k_2, we simulated a physiologically realistic case in which K_1, k_2 both dropped by 15%, i.e., CFB change without V_D change.

A multiple two-sample, one-sided t-test at 0.05 significance level was employed to determine whether the pseudo $\hat{\boldsymbol{F}}^{\boldsymbol{DA}}(t)$ signals, recovered in the presence of CBF change, could be differentiated from *null* signals recovered in the absence of CBF change. A group of 25 "R" and "A" simulated PET signal pairs along with their *null* data counterparts were used for testing. The kinetic parameters, $\overline{\boldsymbol{\theta}}_{\mathrm{tracer}}$, for simulations were chosen

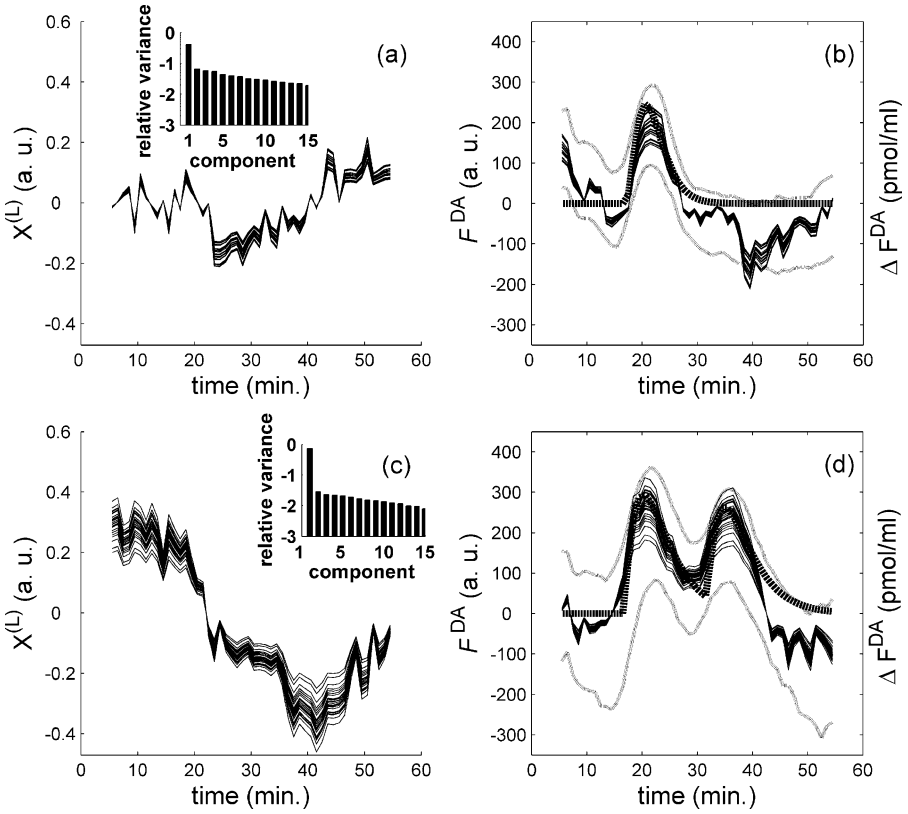

Fig. 2. The recovered activation signals from 25 different simulated PET TACs, representing different voxels, shown in Fig. 1. The upper panels [(a) and (b)] display the recovery of unimodal activation signals and the lower panels [(c) and (d)] show the recovery of bimodal activation. The curves on the left are the rank-L approximation of the activation-only signals, X(L), L $= 1$ (before MMSE filtering) given in arbitrary units (a.u.). The scree plots of relative variances in orthogonal space of the "activation-only" signals, X (log scale) are shown in the inset. The curves on the right are the estimated signals $\hat{\boldsymbol{F}}^{\mathrm{DA}}(t)$ (in a.u., left-hand y-axis) (post MMSE filtering). The thick dotted curves (in pmol/ml, right-hand y-axis) are the true FDA(t) signals used to create the simulation of the activation condition after subtracting the basal concentration. The central 50 min of the recovered signals are displayed in the figure. The thin dotted curves represent the error envelope, extending two standard deviations (point-by-point) above and below the mean estimated $\hat{\boldsymbol{F}}^{\mathrm{DA}}(t)$ curve for the period 5-55 min.

from uniform distributions on an interval $\pm 10\%$ around each canonical value. The mean of the estimated $\hat{\boldsymbol{F}}^{\boldsymbol{DA}}(t)$ signals was compared point-wise (for every time frame) with the mean of similarly estimated *null* $F^{\mathrm{DA}}(t)$ signals. The number of degrees-of-freedom of the t statistics was 23 (25 voxels–2 samples). The alternate hypothesis was that some part (i.e., time points) of the mean of the pseudo $\hat{\boldsymbol{F}}^{\boldsymbol{DA}}(t)$ signals caused by the CBF change should be statistically larger than the mean of the *null* $F^{\mathrm{DA}}(t)$ signals. To be able to perform the t-tests we *forced* the retention of at least one component $(L = 1)$ in the *activation* signals in all cases, disregarding the result of the *scree* plot analysis.

III. Results

A. Recovery of Homogeneous DA Response From Multiple PET Signals

Fig. 1 depicts an instance of 25 noisy TACs simulating the [11C]raclopride kinetics for a study with spatially uniform, time-varying F^{DA}. The top plots represent the TACs under the "R" Fig. 1(a) and "A" Fig. 1(b) conditions created with unimodal F^{DA} activation. The corresponding $F^{\mathrm{DA}}(t)$, used as an input to the compartmental model (see Appendix) is shown below each plot. In the left-hand side bottom half of Fig. 1(a), the straight line represents the assumption that under the "R" condition, DA is constant throughout the scan and is equal to the baseline concentration (100 pmol/ml). The curve in the right-hand side bottom half of Fig. 1(b) illustrates the DA curve used to simulate the "A" state PET signals. DA elevation was initiated at 16.8 min after the start of the scan (i.e., $\tau = 16.8$ min) and reached a peak value at 20.7 min. At its peak, the increase in DA caused 56% occupancy of the receptors. The occupancy is conventionally reported as relative to the available number of receptors at rest. The lower TACs in Fig. 1 correspond to the "R" Fig. 1(c) and "A" Fig. 1(d) signals created using bimodal F^{DA} (shown at bottom, right). In this case, in the "A" state, the DA elevation began 16.8 min after the start of the scan, reached its first peak at 20.2 min, and its second peak at 35.2 min. The occupancy of the receptors reached 60.2% at the first DA peak and 57.2% at the second peak.

Fig. 2 shows the corresponding estimation of DA signals in the two cases of spatially uniform activation. The curves in Fig. 2(a) represent *activation* signals extracted from the 25 pairs of PET signals of the type shown in Fig. 1(a) and Fig. 1(b). In both cases of homogeneous DA response, it was necessary to retain either one or two components of the decomposed "R" signals. One or two components typically accounted for greater

than 99% of the total variance in the $\boldsymbol{R}$ matrix. The bar graph (inset Fig. 2(a)) shows the relative variance of each of the components that result from the decomposition of the difference matrix in (5). Analysis of the bar graph indicated that one component $(\mathrm{L} = 1)$ should be retained in the activation signals for these data. We note that the retained component accounted for 44% of the total variance in $\boldsymbol{X}$. Fig. 2(b) shows the 25 estimates of DA curves, $\hat{\boldsymbol{F}}^{\boldsymbol{DA}}(t)$ following filtering of the 25 curves shown in Fig. 2(a). A MMSE filter with 10 min $(\mathrm{p} = 5)$ kernel width was used. Based on 100 trials of this case with 10% variability in tracer kinetics within a trial and 20% between trials, the estimated DA peak time was 21.7 ± 1.2 min. The true DA change (true $\mathrm{DA\ peak\ time} = 20.7\ \mathrm{min}$) is displayed, for comparison, as the thick dotted line in Fig. 2(b). On the same figure, the thin dotted curves represent the error envelope, which extends two standard deviations above and below the mean estimated DA curve for the period 5–55 min. Fig. 2(c) shows the activation signals derived from the 25 pairs of PET signals created with bimodal F^{DA} activation [see Fig. 1(c) and (d)]. Again, the bar graph [inset Fig. 2(c)], indicates that only one component $(L = 1)$ need be retained from a decomposition of the *difference* signals. The retained component accounts for 73.1% of the total variance in X. The curves in Fig. 2(d) are the $\hat{\boldsymbol{F}}^{\boldsymbol{DA}}(t)$ signals recovered by filtering the signals in Fig. 2(c) with a 10 min $(p = 5)$ wide MMSE filter. The estimated times of the early and late peaks were 22.3 ± 1.6 min and 35.9 ± 1.6 min, respectively. The true DA change curve [thick dotted, Fig. 2(d)] is also shown for comparison.

These figures suggest that we are able to extract a DA signal from dynamic PET data in brain regions in the case where all regions contain a common DA signal, whether unimodal or bimodal. The estimated time of the peak(s) did not vary by much across different voxels (regions) within a given trial (25 "A" + 25 "R" signals) even though each voxel was simulated with different tracer kinetics. We note that within each trial, the estimated time interval between peaks for the recovered bimodal DA signal was preserved. The estimated peak times for these two cases are summarized in Table I.

B. Recovery of Heterogeneous DA Response From Multiple PET Signals

Fig. 3 shows results for analysis of 100 PET signals under both "R" and "A" conditions for which the "A" state was simulated with a "robust" but realistic DA response (peak-to-baseline ratio 8.31:1). The response was initiated at either 20, 25, or 30 min for each set of 25 signals (Table II). The remaining 25 PET signals were *null* data. The 100 estimates of DA curves, $\hat{\boldsymbol{F}}^{\mathrm{DA}}(t)$ are the result of filtering with a 10 min wide filter.

The MMSE filter was the same as that used to analyze the homogeneous activation case. The top three plots [(a)–(c)] depict the extracted DA signals overlaid on their corresponding (dotted) true input DA change curves. The bottom plot [(d)] represents the extracted signals from the *null* data simulations. On this plot, the *null* F^{DA} is represented as a flat dotted line passing through zero (no DA change). Based on 100 trials of 100 voxels each, with 10% variability in tracer kinetics within a trial and 20% between the trials, the mean estimated peak times of the

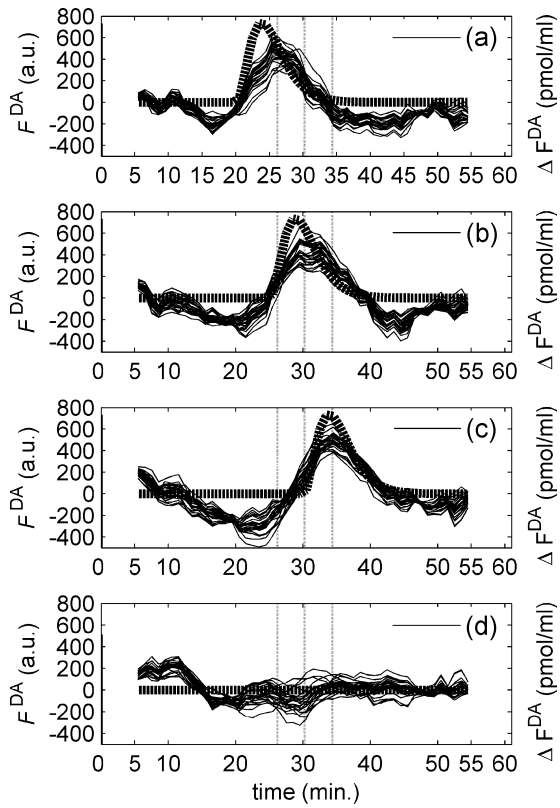

Fig. 3. Example of recovered change in free DA ($\hat{\boldsymbol{F}}^{\mathrm{DA}}(t)$) signals (solid curves, in a.u., left-hand y-axis) from 100 different simulated PET TACs created for "R" and "A" conditions. The TACs were generated with randomly varying tracer kinetic parameters for [11C]raclopride. three sets of 25 "A" state TACs were created with a unique $F^{\mathrm{DA}}(\mathrm{t})$ gamma-variate function (thick dotted lines, in pmol/ml, right-hand y-axis) rising from baseline value at 20, 25, and 30 min, respectively. 25 of the "A" state TACs were created with no DA activation. The signals recovered from the voxels with no activation ("null F^{DA} signals") are plotted in the bottom panel. The plots display the central 50 min of the recovered signals.

DA curves were 26.0 ± 0.7 min, 30.7 ± 0.8 min, and 34.4 ± 0.9 min, respectively. By comparison, the true peak times were 23.8 min, 28.8 min, and 33.8 min. Fig. 4 shows the partition of variances as determined by SVD in (3) and (5) of the rest signals, $\boldsymbol{R}$, and difference signals, X. The *scree* plot in Fig. 4(a) shows the relative variances in the decomposed rest signals, $\boldsymbol{R}$. Based on this plot and the algorithm described in the Section II-C, we retained $K = 2$ components, which accounted for more than 99% of the variance in $\boldsymbol{R}$. In Fig. 4(b), the bar graph shows the contributions to total variance of the difference X signals. Based on this graph, the activation $\boldsymbol{X}^{(\boldsymbol{L})}$ signals were constructed with $L = 4$ significant components. These components accounted each for 44.7%, 13.6%, 4.7%, and 2.9% of the total variance, respectively.

To demonstrate that distinct families of signals can be reliably differentiated, we present a correlation plot for this case. Fig. 5 shows the correlations $\boldsymbol{X}^{(4)}$ of signals with the first singular vector, $\boldsymbol{U}_{X_1}$ versus the correlations of $\boldsymbol{X}^{(4)}$ all signals with the second singular vector, $\boldsymbol{U}_{X_2}$. Note that the clusters allow us to sort the signals according to their distinct temporal features. The 25 recovered signals corresponding to the *null* F^{DA} signals clustered separately from the signals representing true DA activation. The *null* signals represent temporal patterns not related

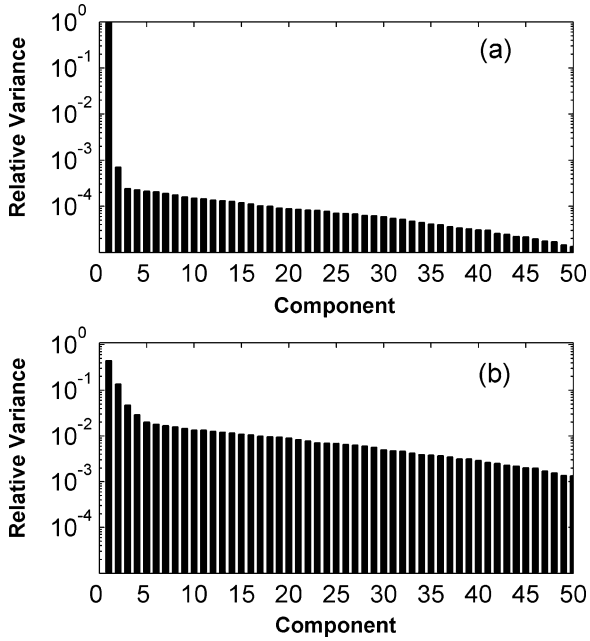

Fig. 4. Scree plots (logarithmic scale) showing the partition of variance of simulated, (a) rest signals, $\mathbf{R}$, and, (b) of activation-only signals, $\mathbf{X}$. Variances correspond to the decompositions leading to the signals shown in Fig. 3. Note three largest singular values [shown in (b)] needed to describe activation signals made up of three different peak times. The fourth singular value accounts for the difference in the initial tracer uptakes between the "R" and "A" scan.

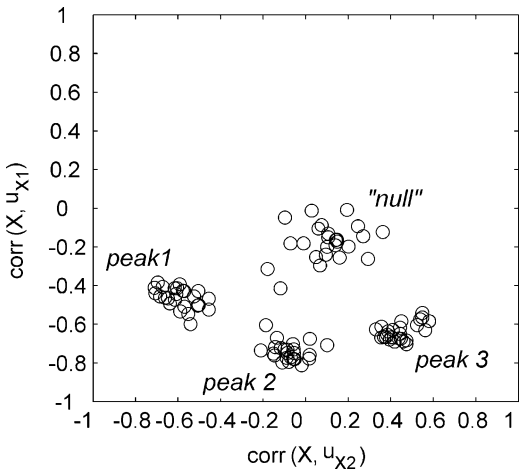

Fig. 5. Correlation of estimated activation-only signals, $\mathbf{X}$, with the first singular vector (component), u_{X_1} versus that with the second, u_{X_2} for the simulated case with the results presented in Fig. 4. The clusters correctly identify four types of temporally distinct components of the data shown in Fig. 4 three activation profiles (corresponding to top three panels) and one family of *null* F^{DA} signals. Peak 1 refers to early, peak 2 refers to middle, and peak 3 refers to late peaking $F^{\mathrm{DA}}(\mathrm{t})$ signals.

to DA activation. This example suggests that we are able to discriminate between voxels that display temporarily distinct DA activation patterns, including differentiating bona fide activation from absence of activation.

Two more cases (see Table II) of simulated spatially heterogeneous activation were considered. The second case, deemed "mild" DA activation (Case 2, Table II), used true DA curves of lower magnitude (peak-to-baseline ratio 3.45:1) than in the first

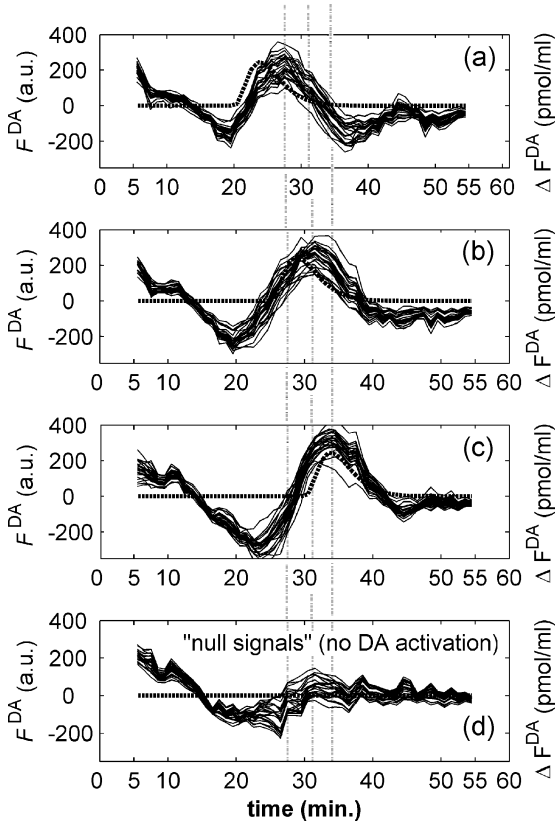

Fig. 6. Example of recovered change in free DA ($\hat{F}^{\mathrm{DA}}(t)$) signals (solid curves, in a.u., left-hand y-axis) from 100 different simulated PET TACs created for "R" and "A" conditions. The TACs were generated with randomly varying tracer kinetic parameters for [11C]raclopride. three sets of 25 "A" state TACs were created with a unique $F^{\mathrm{DA}}(\mathrm{t})$ gamma-variate function (thick dotted lines, in pmol/ml, right-hand y-axis) rising from baseline value at 20, 25 and 30 min, respectively. Twenty-five of the "A" state TACs were created with no DA activation. The signals recovered from the voxels with no activation ("null F^{DA} signals") are plotted in the bottom panel. The plots display the central 50 min of the recovered signals. The vertical lines mark the location of the mean estimated peak times for each distinct group of five signals.

case (described in Figs. 3–5). The 100 estimates of DA curves, $\hat{\boldsymbol{F}}^{\boldsymbol{DA}}(t)$, following filtering with a 10 min wide filter, are shown in Fig. 6. In this case, we retained $L = 3$ significant components in the activation $\boldsymbol{X}^{(\boldsymbol{L})}$ signals. The retained components accounted each for 27.4%, 8.5%, and 4.6% of the total variance, respectively. The fourth component, which accounted for 3.3% of the variance, was not retained. A correlation plot (not shown) of $\boldsymbol{X}^{(3)}$ signals with the first singular vector, $\boldsymbol{U}_{X_1}$ versus the correlations of all $\boldsymbol{X}^{3)}$ signals with the second singular vector, $\boldsymbol{U}_{X_2}$ did not separate the signals into distinct clusters.

A third case (Case 3, Table II), also of "mild" DA activation, was created from DA curves separated by 10 min. In this case, we retained $L = 4$ components in the activation $\boldsymbol{X}^{(\boldsymbol{L})}$ signals with the components accounting for 24%, 11%, 5.9%, and 3.9% of the total variance ($\hat{\boldsymbol{F}}^{\mathrm{DA}}(t)$ estimates not shown). As in the second case, a correlation plot (also not shown) did not present a clear separation between signals representing distinct patterns of activation nor between those signals and no response. The first two recovered DA responses were temporarily distinct, while the third response, occurring late in the scan was not clearly distinct from the cluster representing the null signals.

C. Effects of CBF Change

The apparent activation caused by an unequal drop in K_1 and k_2 (decrease in V_D) values proved to be significant ($p < 0.05$) between 16 min and the end of the scan (i.e., during the entire period of altered blood flow). By contrast, any apparent activation caused by an *equal* drop in both K_1 and k_2 (no change in V_D) was not statistically significant (data not shown). It is important to note that the analysis of the *scree* plot according to the procedure described in the Methods indicated that no component should be retained in the activation signals for both the *null* case and the case of no change in V_D. In contrast, the analysis of the case with decrease in V_D revealed one significant component associated with the pseudo $\hat{\boldsymbol{F}}^{\boldsymbol{DA}}(t)$ signals.

D. Experimental Results

The analysis of our human PET data set revealed two major components in the difference signals. All NAcc and caudate regions in the left hemisphere and all putamen regions in the right hemisphere produced a distinct and similar response. An example of such response is shown in Fig. 7. The recovered DA signal shown is from the left NAcc of the brain of a human subject undergoing IV alcohol infusion after being presented alcohol cues. The MMSE filter that was used previously with the simulated data was also applied to the human activation signals. The $\hat{\boldsymbol{F}}^{\mathrm{DA}}(t)$ curve (dashed line) recovered by $nt\mathrm{PET}$ [19] is presented as percentage of the baseline value, and is shown for comparison with the result of the present nonparametric method. Note that the time of the peak response detected with the nonparametric method precedes the model-based finding by about 2 min. This difference is consistent with test results based on applying both methods to simulated data. In the current paper a bias of about 1 min was found in the recovery of peak time of a single DA response, whereas $nt\mathrm{PET}$ showed a bias of about 3 min when applied to comparable test data [36]. The model-based method produces a smooth prediction of $\boldsymbol{F}^{\mathrm{DA}}(t)$ because it specifies a functional form that is smooth. We also note a few smaller negative peaks that could represent theoretically either a decrease in dopamine concentration or just the effect of increased noise during the late part of the scan.

IV. Discussion

In this study, we demonstrate a new application of singular value decomposition to extract temporal patterns of neurotransmitter change from pairs of dynamic PET data sets acquired under different conditions. Our long term goal is to recover temporal features of the response of a neurotransmitter to a drug challenge. The system of a neurotransmitter in competition with a PET tracer at a limited number of binding sites is inherently nonlinear; nevertheless the application of a linear technique appears to be a fruitful exercise. By making use of two PET scans, we make the implicit assumption that the "R" PET signals contain all the information in the "A" signals that is not related to DA activation. Using linear algebra, this assumption was implemented by retaining the components of the "A" signals that are orthogonal to the "R" subspace determined by the SVD of the R signals.

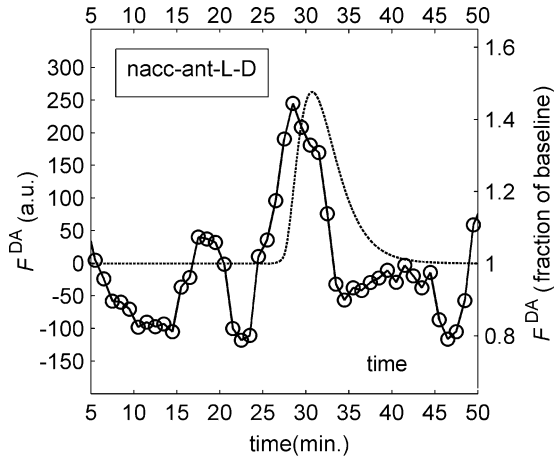

Fig. 7. Estimate of alcohol-induced $\hat{\boldsymbol{F}}^{\mathrm{DA}}(t)$ in a human subject's nucleus accumbens (solid curve, with open circles, in a.u.). Overlaid dashed curve is the $F^{\mathrm{DA}}(t)$ estimate using a parametric approach ($nt\mathrm{PET}$) [19]. The parametric approach yields data in terms of fraction of baseline (right-hand y axis).

We determined that the difference signals must be proportional to the integral of the F^{DA} time course. The major components of the difference, referred to as *activation*, suggested that a derivative-like operator applied to the activation signals would provide a good approximation to the $F^{\mathrm{DA}}(t)$ profile. The need for a derivative can also be inferred from previous simulation studies of 11Craclopride uptake by Endres and Carson [11], [12]. They demonstrated that the decrease in tracer concentration in the tissue due to the binding of DA to receptors is linearly proportional to the integral of the $F^{\mathrm{DA}}(t)$ curve. Instead of a simple derivative, we chose to design an MMSE filter to perform the derivative-like operation without amplifying the noise. The advantages of using a MMSE filter are that it can be designed by training with data that behaves in a predictable way, and it performs well on noisy data. The scale of the MMSE filter is largely dependent on the choice of kinetic rate constants for the simulation of training data and less on the scale of the F^{DA} functions. Ideally, the filter would need to be retrained if it were to be applied to signals from a displaceable tracer with kinetics substantially different than those of [11C]raclopride.

A. Recovering Neurotransmitter Timing (Homogeneous Activation)

We first tested our algorithm on a simple case in which a small group of simulated voxels in the "A" condition were characterized by a single DA response. The simulated voxels took into account intrasubject variation in PET tracer kinetics. Despite this variation, we were able to recover F^{DA} takeoff and the peak times precisely. Two peaks of a bimodal DA pattern could also be recovered precisely. In the bimodal case, both the time interval between the peaks and the ratio of their heights were preserved. The observed variance in the detected peak times appears to be introduced by the noise and not by variation in tracer kinetics. On one hand, analysis of simulations containing kinetic variation but no noise produces variation in scale but no variation in the peak time across voxels. On the other hand, noisy data with unchanging tracer parameters produces variable peak times across voxels. These findings suggest that the method will

be robust in the face of naturally occurring variation in tracer kinetics across brain regions.

B. Heterogeneous Timing Recovered

We also demonstrated, in a less idealized scenario, that one can discriminate and identify multiple different time-varying DA responses. In fact, at the noise level present in our simulations, DA responses separated by as little as 5-min intervals could be distinguished. In separate, noise-free simulations, not reported in this paper, responses separated by as little as 1 min could be separated. There was a consistent bias between the true and detected peak times and this bias appears to be largest at early times. Further investigation is needed to determine the source of this bias. In the case of strong DA activations separated by 5-min time intervals, a correlation plot was definitive in identifying temporarily distinct peaks. Mild signals that were inadequately spaced in time could not be definitively separated via the correlation plot. However, in all three cases of heterogeneous activation, our analysis recovered groups of DA peaks that were easily distinguished visually.

C. No Absolute Scale Recovered

We were unable to recover the absolute scale of the F^{DA} change. The effect of the DA change on the PET measurement is due to competition between the DA and the tracer. Competition is a bimolecular and saturable process which is inherently nonlinear [see interaction term in (A3)]. Under conditions of prolonged receptor saturation we cannot hope to recover the proper scale of the F^{DA} signal. Below saturation, by using the MMSE filter, we had hoped to recover the scale of the F^{DA}. Unfortunately, the MMSE filter itself is a function of tracer parameters of the training set [expressed in (7)]. Applying the proper training set would require *a priori* knowledge of the true tracer parameters which, in practice, will not be known. The filter used for the results in Fig. 2 and 3 was designed from training data whose tracer parameters were taken from the same distribution as the test data (e.g., Fig. 1). This explains why our recovered DA signals appear properly scaled. Nevertheless, it appears that DA timing information is preserved.

In simulations, we used a larger value for kinetic parameter K_1 $(= 0.448\ \mathrm{ml/min/g})$ than that reported in literature [6], [37], which is around 0.1 ml/min/g. We did so to be consistent with our experimental data. However, the main effect of K_1 is to scale the entire TAC; it is not related to the relative changes in binding caused by DA activation [12]. By a simple analysis of (4) we can asses that K_1 will impact the scale of the *difference* signals, X, mainly through its effect on PET signals contained in matrix A. The matrix $(\boldsymbol{I}-\boldsymbol{U}_R^{(K)}\cdot\boldsymbol{U}_R^{(K)^T})$ has norm 1 and it is not expected to impact the scale of X, as much as A. Following this argument, we can infer that if we use a lower K_1 value, the recovered $F^{\mathrm{DA}}(t)$ signal would only be scaled down. In fact, we tested this hypothesis for the unimodal case by simulating with a value of K_1 of 0.092 ml/min/g (as in [6]) and keeping the other kinetic parameters as described herein. We were able to recover the same shape of response and the timing as in the example shown in Fig. 2(b). However, as expected, the magnitude of the $F^{\mathrm{DA}}(t)$ signal was underestimated with respect to the true. We also note that our value for k_2 $(= 0.4326\ \mathrm{min}^{-1})$ was comparable to that in literature [6], even though one might expect that, an estimation that produces a large value for K_1 would produce a high value for k_2. One possible explanation for high K_1 but moderate k_2 is that we did not account for nonspecific binding when we modeled our TACs.

In separate simulations, we have tested the case of two scans differing in injected doses by a factor of 2. The scale of the recovered signals remained unchanged. This demonstrates that the estimation of the difference signals is unaffected by a difference in the injected doses between the "R" and "A" scans.

D. Blood Flow Changes Will not Cause False F^{DA}

We specifically addressed possible confounds that could be caused by changes in mean CBF between the "R" and "A" scan. Previous studies with single photon emission computed tomography (SPECT) have reported reductions in blood flow in several brain regions, following administration of cocaine [38], [39]. Volkow *et al.* demonstrated reduced blood flow in the cerebellum following acute alcohol intoxication [40]. If such findings of decreased blood flow were to be demonstrated in DA rich striatal regions, then these might represent a possible confound. To address our concerns, we investigated the possibility of false findings being caused by changes in CBF. We showed that simultaneous but unequal drops in K_1, and k_2 from "R" to "A" states, may lead to false F^{DA} responses. This result is consistent with other findings [6], [19], [41]. Nonetheless, as others have stated, a transient change in V_D is physiologically implausible. When we tested a more plausible case, of equal drop in K_1 and k_2, we detected no significant F^{DA} signal.

E. Advantages of the Method

A major advantage of our approach is that it is data driven. We assume that the difference between the "R" and "A" conditions could be attributed solely to increases in neurotransmitter concentration. In addition, the nature of the SVD is to assume that activation is added linearly to the baseline state. More importantly, because it is nonparametric, the method does not require any *a priori* knowledge of the functional form of the F^{DA} signal. The method might also be used in conjunction with a model-based approach as a prescreening procedure to determine a reasonable parameterization for $F^{\mathrm{DA}}(t)$ that could then be used for subsequent parameter estimation. Our approach does not require arterial blood sampling and thus removes a serious impediment to routine application to human PET studies.

F. Limitations

1) Artifacts: Let us consider the limitations of this method. The analysis of our signal estimates revealed inaccurate recovery of the true F^{DA} at the beginning of the time course. There is a consistent undershoot/overshoot, in the earliest section of the data, preceding the takeoff of the true DA. We believe that this effect is caused by the initial tracer uptake from the systemic circulation to the free compartment. From our studies we observed that the shape of the exogenous input, $P(t)$ influences the shape of the extracted DA signals at early time. This artifact argues against the recovery of DA responses that occur very early in a PET study. As a precaution, we decided

to discard the first 5 min of each estimated $\hat{F}^{\mathrm{DA}}(t)$ signal. As a possible experimental amelioration of this artifact, we propose that a tracer be delivered as constant infusion initiated before the start of the scan. This procedure should favor the artifact-free recovery of DA signals and allow the DA release stimulus be applied at anytime during the "A" scan.

The difference in the initial uptake of tracer into the tissue during the "R" and "A" scans introduces an additional confound in the form of slowly time-varying signals. This behavior can be viewed in the recovered *null* F^{DA} signals in Fig. 3(d). In the absence of the true DA signals, the fourth component of the activation signals, $\boldsymbol{X}^{(4)}$, accounts mostly for these signals. The confound was introduced by using different exogenous input curves, $P(t)$, to generate realistic TACs for the "R" and "A" conditions (see Fig. 9). The confound is eliminated if a single $P(t)$ input is used both for "R" and "A". One possible solution for reducing the impact of this confound may be further post-processing. In the future, in order to minimize the confounding effects, we may consider rotation of the computed singular vectors in the reduced subspace spanned by the most significant components of activation.

The recovered signals tend to take on negative values immediately before and after the peak. Negative values preceding the pulse are primarily due to effects of the MMSE filter, which adds a negative offset. Negative values following the recovered pulse result from the possible presence of nonlinear terms in the relationship between the difference signals, X and the true integral of the F^{DA} time course. One of our premises for our analysis method is that this relationship is linear.

2) Temporal Resolution Limitations: The simulated PET signals were based on 1-min time frames, which established a lower limit for the temporal resolution. The sampling rate is determined in practice by the dynamic PET acquisition protocol to balance signal-to-noise ratio (SNR), temporal sensitivity, and data management. In addition to data sampling, the noise in the PET data also limits the temporal resolution. Further improvements in SNR and in the sensitivity of PET data acquisition may make it possible to achieve better temporal resolution of the estimated signals.

The choice of the MMSE filter kernel size can alter the recovery of narrow signal peaks, and therefore affect the temporal resolution. A narrow kernel will not perform well on noisy estimates. A wide kernel, will dampen down signal peaks narrower than the kernel width, and merge peaks that are closer together in time than the kernel width. It appears that MMSE filter is best able to recover signal peaks with full-width at half-maximum (FWHM) equal to half the kernel size. In the work presented here, we used a 10 min wide filter. Given the noise level in our data, we could satisfactorily recover signals containing peaks with at least 5 min FWHM. At the expense of reducing the SNR, we can adjust the filter kernel width to preserve narrower peaks.

3) Sensitivity Limitations: There are two factors that may limit the sensitivity of the method to weak DA activation occurring towards the end of a scan with [11C]raclopride delivered as bolus. First, the noise level is high during the latter part of the 1-h scan, when there is less activity due to the short half-life of C-11 tracers. Second, the amount of free tracer available for competition with the endogenous DA also decreases in time due to the clearance of tracer from the tissue. These limitations may have been at work in heterogeneous activation Case 3. Signals with DA peaking late in time could not be distinguished from the signals with no activation via correlation plots.

The choice of 25–100 TACs in our simulations was arbitrary and does not indicate either an upper or lower limit for the extraction of $F^{\mathrm{DA}}(t)$ signals. There is no *a priori* limitation to the number of independent PET signals that can/must be used. However, in order to separate all the components contained in the signals, the number of signals must be at least equal to the number of components. Intuitively, we expect the following factors would place practical limits on the minimum number of PET signals required for analysis: 1) noise, 2) strength of the activation, and 3) number of distinct activation components in the data.

G. Possible Applications

The most encouraging result presented here is our ability to discern one or more temporal signatures of activation within a brain region. The recovery of a bimodal pattern of activation is exciting because it portends the application of our method to data analysis from complicated, multi-component neurophysiological imaging studies. For example, drug-taking behavior, which is known to be related to the dopamine system, may be caused by multiple environmental cues and other chemical stimuli (e.g., nicotine or alcohol). A researcher interested in studying interaction of drugs and environment, may want to use PET to asses the dopaminergic response to a sequence of stimuli which could be bimodal or even multimodal. The ability of this method to recover spatially heterogeneous patterns of activation via simple matrix computations could offer the possibility of studying related sequences of neurochemical events. In this study, we applied our method to the neurotransmitter dopamine and the ligand [11C]raclopride. However, we believe that this method could be easily extended to other displaceable ligands to study other neurotransmitter systems. We note that we analyzed simulations of more slowly dissociating tracers (e.g. [18F]fallypride) and the method was able to extract useful time information.

V. Conclusion

We have designed a non-parametric technique that can extract temporal information about neurotransmitter change in the brain from dynamic PET data. Our method shows potential for separating temporarily different dopaminergic responses, and we suggest its use for the study of regional and brain-wide dynamics of neurotransmitter systems. Based on simulations with appropriate noise levels, we believe this method may be robust enough for use at the voxel level.

Appendix

A. The Enhanced Model Equations

The compartmental model shown pictorially in Fig. 8 is described by a system of differential equations that represent mass

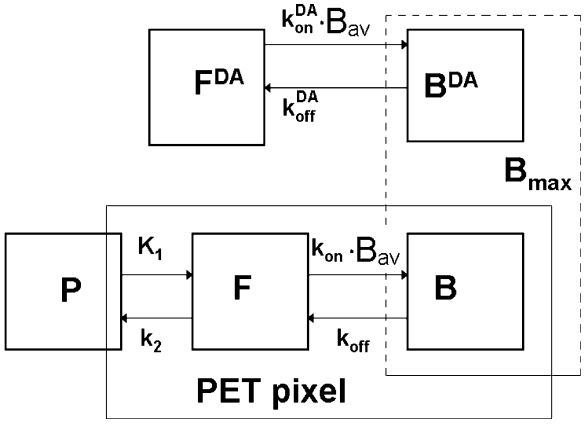

Fig. 8. Enhanced compartmental ligand-receptor model used for the data simulation. P represents the plasma input, F and B are the free and bound tracer compartments. F^{DA} is the free endogenous dopamine input and B^{DA} is the bound dopamine compartment. $\mathrm{B}_{\max}$ denotes the maximum concentration of available receptor binding sites (dashed rectangle around B and B^{DA}) for which DA and the tracer can compete. The solid rectangle around F, B and part of P shows the relative contribution of each compartment to a PET measurement at any given time. B_{av} stands for the available binding sites. P, F, B, F^{DA}, B^{DA}, and B_{av} are time varying, K_1, k_2, k_{on}, $B_{\max}$, k_{off}, $k_{\mathrm{on}}^{\mathrm{DA}}$, and $k_{\mathrm{off}}^{\mathrm{DA}}$ are constants.

balances. The balance equation for the free tracer, $F(t)$ in molar quantities is

$$\frac{dF(t)}{dt} = K_1 \cdot P(t) - k_2 \cdot F(t) - k_{\mathrm{on}} \cdot \left[B_{\max} - B(t) - B^{\mathrm{DA}}(t)\right] \cdot F(t) + k_{\mathrm{off}} \cdot B(t). \quad \text{(A1)}$$

The balance equation for the bound tracer, $B(t)$ is:

$$\frac{dB(t)}{dt} = k_{\mathrm{on}} \cdot \left[B_{\max} - B(t) - B^{\mathrm{DA}}(t)\right] \cdot F(t) - k_{\mathrm{off}} B(t). \quad \text{(A2)}$$

The balance equation for the endogenous DA, $B^{DA}(t)$ is

$$\frac{dB^{\mathrm{DA}}(t)}{dt} = k_{\mathrm{on}}^{\mathrm{DA}} \cdot \left[B_{\max} - B(t) - B^{\mathrm{DA}}(t)\right] \cdot F^{\mathrm{DA}}(t) - k_{\mathrm{off}}^{\mathrm{DA}} B^{\mathrm{DA}}(t). \quad \text{(A3)}$$

The exogenous tracer kinetics are described by the compartments for the free and specifically bound tracer in tissue. There are four unknown kinetic parameters for the tracer: K_1 and k_2, the influx/efflux rate constants between the plasma and the free ligand compartment; and k_{on} and k_{off}, the ligand association and dissociation rate constants, respectively. $B_{\max}$, the total receptor density, is also specified in the equations. $P(t)$, the instantaneous molar concentration of tracer in plasma, can be regarded as the tracer input to the system. The other two time dependent variables $F(t)$, $B(t)$ represent the instantaneous molar concentration of tracer in free and bound compartments, respectively. The endogenous ligand is accounted for by one additional compartment (bound DA) and its kinetics are described by two additional kinetic parameters: $k_{\mathrm{on}}^{\mathrm{DA}}$, and $k_{\mathrm{off}}^{\mathrm{DA}}$, the association and dissociation rate constants for the endogenous ligand (i.e., DA). $F^{\mathrm{DA}}(t)$, the free DA concentration in the synapse

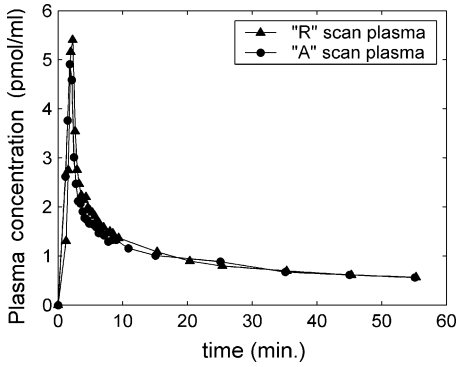

Fig. 9. Bolus plasma curves used in simulations. The curves were derived from measured blood curves in a human PET experiment with [11C]raclopride. The scans were conducted with the subject at rest (filled triangles) and under a stimulus condition (filled circles).

is an additional input to the system, which was simulated for the purpose of creating test data. $B^{\mathrm{DA}}(t)$ is the instantaneous endogenous dopamine molar concentration in the bound state. Equation (A3) is coupled to the rest of the model through the interaction term, $[B_{\max} - B(t) - B^{\mathrm{DA}}(t)] \cdot F^{\mathrm{DA}}(t)$, which means that binding is a bimolecular and saturable phenomenon that depends on both concentration of available receptors, $B_{av} = [B_{\max} - B(t) - B^{\mathrm{DA}}(t)]$, and free DA, $F^{\mathrm{DA}}(t)$. $P(t)$, used for simulations, was derived from measured blood activity curves. The input plasma curves are shown in Fig. 9. The endogenous input $F^{\mathrm{DA}}(t)$ is simulated using gamma-variate functions, as described in Methods.

B. The PET Curve Output

The (A1)–(A3) were solved numerically for $B(t)$, $F(t)$, and $B^{\mathrm{DA}}(t)$. To do so we used an interactive kinetic modeling package in Matlab that was written in our laboratory using COMKAT, a library of model-related commands that facilitate quick model construction, robust ODE solving, and nonlinear parameter estimation [42]. The kinetic parameter values used in simulations were $K_1 = 0.4486\ \mathrm{ml/min/g}$, $k_2 = 0.4326\ \mathrm{min}^{-1}$, $k_{\mathrm{on}} = 0.01$, $B_{\max} = 55.1093\ \mathrm{pmol/ml}$, $k_{\mathrm{off}} = 0.1409$. These values were estimated from the fitting of a two-tissue compartment model to [11C]raclopride TACs measured from human brain regions with high specific binding. The PET data that were used for estimation of tracer parameters were acquired under the rest condition. The DA association and dissociation rates at D2/D3 receptor sites, $k_{\mathrm{on}}^{\mathrm{DA}} = 25\ \mathrm{ml} \cdot \mathrm{pmol}^{-1} \cdot \mathrm{min}^{-1}$ and $k_{\mathrm{off}}^{\mathrm{DA}} = 0.25\ \mathrm{min}^{-1}$ were taken from a literature review [2] and fixed. The PET measurement of average radioactivity concentration over a single time frame, $[\mathrm{t_s t_e}]$, was constructed as

$$\mathrm{TAC}(t) = \frac{1}{\Delta t} \int_{t_s}^{t_e} \left(\begin{array}{c} F_v C_{\mathrm{blood}}(t) + \\ T_v \left(F(t) + B(t)\right) \cdot SA(t) \end{array} \right) dt + n(t). \quad \text{(A4)}$$

The instantaneous concentrations of the tracer in the blood ($C_{\mathrm{blood}}(t)$) and tissue compartments ($F(t)$ and $B(t)$), are summed in proportion to their respective volume fractions in the voxel or region being measured (F_v for the plasma activity

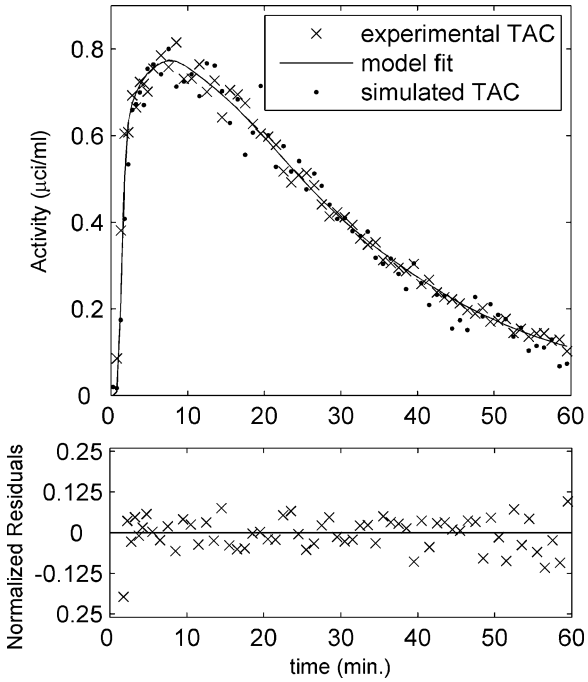

Fig. 10. The upper plot shows an example of voxel data used for estimation of noise variance. The symbol (x) represents a TAC taken from a voxel in the striatum of a subject scanned with [11C]raclopride under the rest condition. The data were fit to a two-tissue compartmental model using an ELS3 cost function. The model fit is shown as a solid curve. An example of simulated data using the estimated variance is also shown (black dots). The lower plot shows the normalized residuals (data-model)/model) of the fitted data.

and $T_v = 1 - F_v$ for the tissue activities). We accounted for intravascular radioactivity by assuming a value of 0.04 for $Fv.SA(t)$ represents the specific activity (in units of activity per mole). It converts the instantaneous tissue concentrations from molar to radioactivity concentrations, and is time-dependent because of radioactive decay. $n(t)$ represents the additive noise term. Because the PET measurement, represented in (A4) is taken over a discrete interval, the instantaneous quantities, on the right, are integrated over the period from time t_s to t_e. The integral is divided by total acquisition frame duration, $\Delta t = t_e - t_s$, to yield the average radioactivity concentration over the frame. For the simulated data, we used a high value of $SA(0) = 1.0\ \mu\mathrm{Ci/pmol}$ at the start of scanning, which is consistent with tracer conditions.

C. Noise Variance Estimation

The parameters $\mathbf{q} = [q_1, q_2, q_3]$ were estimated from our [11C]raclopride data acquired under a rest condition, on a voxel-by-voxel basis from regions with high specific binding. Multiple fits to a two-tissue compartmental model were performed using a variation of the extended least square (ELS) technique [43], [44]. This technique uses an augmented cost function in which the error variance depends explicitly on model parameters. Apart from the four model parameters (kinetic rate constants) of the compartmental model, the cost function included three parameters (referred to as "ELS3" in [42]), $\mathbf{q}$, that describe the variance. In this case we considered the 4 kinetic rate constants as nuisance parameters. Taken individually, the three parameters, $\mathbf{q}$, were not identifiable. Following the multiple fits we retained only those values of $q1$, $q2$, and $q3$ for which the fit was satisfactory based on the examination of normalized residuals. The values of $\mathbf{q}$ from all the retained fits were averaged to yield our estimate of the variance $\sigma^2(t;\mathbf{q}) = q_1 + q_2^*(\mathrm{TAC}(t)/\Delta t)^{q3}$. An example of such a fit is shown in Fig. 10. The estimated values of $\mathbf{q}$ were $q1 = 0.0242$, $q2 = 0.0333$, $q3 = 1.4511$.

ACKNOWLEDGMENT

The authors would like to thank their colleagues Dr. K. Yoder for acquiring the experimental PET data for our analysis and M. Normandin for help with the model-based estimation. They would also like to thank Dr. R. Muzic, for generously supplying Matlab code and advice on the use of the ELS3 model.

REFERENCES

[1] E. D. Morris, R. E. Fisher, N. M. Alpert, S. L. Rauch, and A. J. Fischman, "In vivo imaging of neuromodulation using positron emission tomography: optimal ligand characteristics and task length for detection of activation," *Hum. Brain Mapp.*, no. 3, pp. 35–55, 1995.

[2] R. E. Fisher, E. D. Morris, N. M. Alpert, and A. J. Fischman, "*In vivo* imaging of neuromodulatory synaptic transmission using PET: A review of relevant neurophysiology," *Hum. Brain Mapp.*, no. 3, pp. 24–34, 1995.

[3] M. Laruelle, R. N. Iyer, M. S. al Tikriti, Y. Zea-Ponce, R. Malison, S. S. Zoghbi, R. M. Baldwin, H. F. Kung, D. S. Charney, P. B. Hoffer, R. B. Innis, and C. W. Bradberry, "Microdialysis and SPECT measurements of amphetamine-induced dopamine release in nonhuman primates," *Synapse*, vol. 25, no. 1, pp. 1–14, Jan. 1997.

[4] R. E. Carson, A. Breier, A. de Bartolomeis, R. C. Saunders, T. P. Su, B. Schmall, M. G. Der, D. Pickar, and W. C. Eckelman, "Quantification of amphetamine-induced changes in [11C]raclopride binding with continuous infusion," *J. Cereb. Blood Flow Metab.*, vol. 17, no. 4, pp. 437–447, Apr. 1997.

[5] M. J. Koepp, R. N. Gunn, A. D. Lawrence, V. J. Cunningham, A. Dagher, T. Jones, D. J. Brooks, C. J. Bench, and P. M. Grasby, "Evidence for striatal dopamine release during a video game," *Nature*, vol. 393, no. 6682, pp. 266–268, May 1998.

[6] S. Pappata, Dehaene, J. B. Poline, M. C. Gregoire, A. Jobert, J. Delforge, V. Frouin, M. Bottlaender, F. Dolle, L. Di Giamberardino, and A. Syrota, "In vivo detection of striatal dopamine release during reward: A PET study with [(11)C]raclopride and a single dynamic scan approach," *Neuroimage*, vol. 16, no. 4, pp. 1015–1027, Aug. 2002.

[7] R. D. Badgaiyan, A. J. Fischman, and N. M. Alpert, "Striatal dopamine release during unrewarded motor task in human volunteers," *Neuroreport*, vol. 14, no. 11, pp. 1421–1424, Aug. 2003.

[8] A. Breier, T. P. Su, R. Saunders, R. E. Carson, B. S. Kolachana, A. de Bartolomeis, D. R. Weinberger, N. Weisenfeld, A. K. Malhotra, W. C. Eckelman, and D. Pickar, "Schizophrenia is associated with elevated amphetamine-induced synaptic dopamine concentrations: Evidence from a novel positron emission tomography method," *Proc. Natl. Acad. Sci. USA*, vol. 94, no. 6, pp. 2569–2574, Mar. 1997.

[9] N. Ginovart, L. Farde, C. Halldin, and C. G. Swahn, "Effect of reserpine-induced depletion of synaptic dopamine on [11C]raclopride binding to D2-dopamine receptors in the monkey brain," *Synapse*, vol. 25, no. 4, pp. 321–325, Apr. 1997.

[10] K. K. Yoder, C. Wang, and E. D. Morris, "Change in binding potential as a quantitative index of neurotransmitter release is highly sensitive to relative timing and kinetics of the tracer and the endogenous ligand," *J. Nucl. Med.*, vol. 45, no. 5, pp. 903–911, May 2004.

[11] C. J. Endres, B. S. Kolachana, R. C. Saunders, T. Su, D. Weinberger, A. Breier, W. C. Eckelman, and R. E. Carson, "Kinetic modeling of [11C]raclopride: Combined PET-microdialysis studies," *J. Cereb. Blood Flow Metab.*, vol. 17, no. 9, pp. 932–942, Sep. 1997.

[12] C. J. Endres and R. E. Carson, "Assessment of dynamic neurotransmitter changes with bolus or infusion delivery of neuroreceptor ligands," *J. Cereb. Blood Flow Metab.*, vol. 18, no. 11, pp. 1196–1210, Nov. 1998.

[13] K. J. Friston, A. L. Malizia, S. Wilson, V. J. Cunningham, T. Jones, and D. J. Nutt, "Analysis of dynamic radioligand displacement or "activation" studies," *J. Cereb. Blood Flow Metab.*, vol. 17, no. 1, pp. 80–93, Jan. 1997.

[14] R. N. Gunn, A. A. Lammertsma, S. P. Hume, R. Myers, P. M. Bloomfield, and V. J. Cunningham, "A simplified reference region approach to parametric imaging of ligand receptor binding in PET," *J. Nucl. Med.*, vol. 38, no. 5, p. 875, May 1997.

[15] N. M. Alpert, R. D. Badgaiyan, E. Livni, and A. J. Fischman, "A novel method for noninvabsive detection of neuromodulatory changes in specific neurotransmitter systems," *Neuroimage*, vol. 19, no. 3, pp. 1049–1060, July 2003.

[16] A. A. Grace, "The tonic/phasic model of dopamine system regulation and its implications for understanding alcohol and psychostimulant craving," *Addiction*, vol. 95, pp. S119–S128, Aug. 2000.

[17] N. D. Volkow, Y. S. Ding, J. S. Fowler, G. J. Wang, J. Logan, J. S. Gatley, S. Dewey, C. Ashby, J. Liebermann, and R. Hitzemann, "Is methylphenidate like cocaine? Studies on their pharmacokinetics and distribution in the human brain," *Arch. Gen. Psych.*, vol. 52, no. 6, pp. 456–463, Jun. 1995.

[18] N. D. Volkow and J. M. Swanson, "Variables that affect the clinical use and abuse of methylphenidate in the treatment of ADHD," *Amer. J Psych.*, vol. 160, no. 11, pp. 1909–1918, Nov. 2003.

[19] E. D. Morris, K. K. Yoder, C. Wang, M. D. Normandin, Q. H. Zheng, B. Mock, R. F. Muzic, Jr., and J. C. Froehlich, "ntPET: A new application of PET imaging for characterizing the kinetics of endogenous neurotransmitter release," *Mol. Imag.*, vol. 4, no. 4, pp. 473–489, Oct. 2005.

[20] G. H. Golub and C. F. Van Loan*, Matrix Computation*, 3rd ed. Baltimore, MD: Johns Hopkins Univ. Press, 1996.

[21] K. J. Friston, C. D. Frith, P. F. Liddle, and R. S. J. Frackowiak, "Functional connectivity—the principal-component analysis of large (pet) data sets," *J. Cereb. Blood Flow Metabol.*, vol. 13, no. 1, pp. 5–14, Jan. 1993.

[22] K. J. Worsley, "An overview and some new developments in the statistical analysis of PET and fMRI data," *Hum. Brain Mapp.*, vol. 5, no. 4, pp. 254–258, 1997.

[23] K. J. Friston, J. B. Poline, A. P. Holmes, C. D. Frith, and R. S. J. Frackowiak, "A multivariate analysis of PET activation studies," *Hum. Brain Mapp.*, vol. 4, no. 2, pp. 140–151, 1996.

[24] A. H. Andersen, D. M. Gash, and M. J. Avison, "Principal component analysis of the dynamic response measured by fMRI: A generalized linear systems framework," *Magn. Resonan. Imag.*, vol. 17, no. 6, pp. 795–815, Jul. 1999.

[25] C. W. Bradberry, "Acute and chronic dopamine dynamics in a nonhuman primate model of recreational cocaine use," *J. Neurosci.*, vol. 20, no. 18, pp. 7109–7115, Sep. 2000.

[26] H. Tsukada, N. Harada, S. Nishiyama, H. Ohba, and T. Kakiuchi, "Dose-response and duration effects of acute administrations of cocaine and GBR12909 on dopamine synthesis and transporter in the conscious monkey brain: PET studies combined with microdialysis," *Brain Res.*, vol. 860, no. 1–2, pp. 141–148, Mar. 2000.

[27] K. Yoshimoto, W. J. McBride, L. Lumeng, and T. K. Li, "Alcohol stimulates the release of dopamine and serotonin in the nucleus accumbens," *Alcohol*, vol. 9, no. 1, pp. 17–22, Jan. 1992.

[28] K. K. Yoder, D. A. Kareken, R. A. Seyoum, S. J. O'Connor, C. Wang, Q. H. Zheng, B. Mock, and E. D. Morris, "Dopamine D(2) receptor availability is associated with subjective responses to alcohol," *Alcohol Clin. Exp. Res.*, vol. 29, no. 6, pp. 965–970, June 2005.

[29] S. O'Connor, S. Morzorati, J. Christian, and T. K. Li, "Clamping breath alcohol concentration reduces experimental variance: Application to the study of acute tolerance to alcohol and alcohol elimination rate," *Alcohol Clin. Exp. Res.*, vol. 22, no. 1, pp. 202–210, Feb. 1998.

[30] D. A. Kareken, E. D. Claus, M. Sabri, M. Dzemidzic, A. E. Kosobud, A. J. Radnovich, D. Hector, V. A. Ramchandani, S. J. O'Connor, M. Lowe, and T. K. Li, "Alcohol-related olfactory cues activate the nucleus accumbens and ventral tegmental area in high-risk drinkers: preliminary findings," *Alcohol Clin. Exp. Res.*, vol. 28, no. 4, pp. 550–557, Apr. 2004.

[31] C. Heidbreder and P. De Witte, "Ethanol differentially affects extracellular monoamines and GABA in the nucleus accumbens," *Pharmacol. Biochem. Behav.*, vol. 46, no. 2, pp. 477–481, Oct. 1993.

[32] I. Boileau, J. M. Assaad, R. O. Pihl, C. Benkelfat, M. Leyton, M. Diksic, R. E. Tremblay, and A. Dagher, "Alcohol promotes dopamine release in the human nucleus accumbens," *Synapse*, vol. 49, no. 4, pp. 226–231, Sep. 2003.

[33] J. Jackson*, A Users Guide to Principal Components*. New York: Wiley, 1991.

[34] N. Wiener*, Extrapolation, Interpolation and Smoothing of Stationary Time Series With Engineering Applications*. New York: Wiley, 1949.

[35] D. P. Berrar, W. Dubitzky, and M. Granzow, "Singular value decomposition and principal component analysis," in *A Practical Approach to Microarray Data Analysis*. Boston, MA: Kluwer Academic, 2003, pp. 91–109.

[36] M. D. Normandin and E. D. Morris, "Temporal resolution of ntPET using either arterial or reference region-derived plasma input functions," in *Proc. 28th Annu. IEEE Conf. Eng. Med. Biol.*, New York, 2006, pp. 2005–2008.

[37] L. Farde, L. Eriksson, G. Blomquist, and C. Halldin, "Kinetic analysis of central [11C]raclopride binding to D2-dopamine receptors studied by PET—A comparison to the equilibrium analysis," *J. Cereb. Blood Flow Metab.*, vol. 9, no. 5, pp. 696–708, Oct. 1989.

[38] B. Johnson, L. Lamki, B. Fang, B. Barron, L. Wagner, L. Wells, P. Kenny, D. Overton, S. Dhother, D. Abramson, R. Chen, and L. Kramer, "Demonstration of dose-dependent global and regional cocaine-induced reductions in brain blood flow using a novel approach to quantitative single photon emission computerized tomography," *Neuropsychopharmacology*, vol. 18, no. 5, pp. 377–384, May 1998.

[39] E. A. Wallace, G. Wisniewski, G. Zubal, C. H. vanDyck, S. E. Pfau, E. O. Smith, M. I. Rosen, M. C. Sullivan, S. W. Woods, and T. R. Kosten, "Acute cocaine effects on absolute cerebral blood flow," *Psychopharmacology (Berl)*, vol. 128, no. 1, pp. 17–20, Nov. 1996.

[40] N. D. Volkow, N. Mullani, L. Gould, S. S. Adler, R. W. Guynn, J. E. Overall, and S. Dewey, "Effects of acute alcohol intoxication on cerebral blood flow measured with PET," *Psych. Res.*, vol. 24, no. 2, pp. 201–209, May 1988.

[41] A. Dagher, R. Gunn, G. Lockwood, V. J. Cunningham, and P. M. Grasby, , R. Carson, M. Daube-Witherspoon, and P. Herscovitch, Eds., "Measuring neurotransmitter release with Positron Emission Tomography: Methodological issues," in *Quantitative Functional Brain Imaging with Positron Emission Tomography*. San Diego, CA: Academic, 1998, pp. 449–454.

[42] R. F. Muzic, Jr. and S. Cornelius, "COMKAT: compartment model kinetic analysis tool," *J. Nucl. Med.*, vol. 42, no. 4, pp. 636–645, Apr. 2001.

[43] C. C. Peck, S. L. Beal, L. B. Sheiner, and A. I. Nicholas, "Extended least squares nonlinear regression: A possible solution to the "choice of weights" problem in analysis of individual pharmacokinetic data," *J. Pharmacokinet Biopharm.*, no. 12, pp. 545–548, 1984.

[44] R. F. Muzic, Jr. and B. T. Christian, "Evaluation of objective functions for estimation of kinetic parameters," *Med. Phys.*, vol. 33, no. 2, pp. 342–353, Feb. 2006.